

2011 Special Issue

The pedunculopontine nucleus as an additional target for deep brain stimulation

M.A.J. Lourens ^{a,c,*}, H.G.E. Meijer ^{a,c}, T. Heida ^{b,c}, E. Marani ^{b,c}, S.A. van Gils ^{a,c}^a Department of Applied Mathematics, University of Twente, Enschede, 7500 AE, The Netherlands^b Department of Electrical Engineering, University of Twente, Enschede, 7500 AE, The Netherlands^c MIRA: Institute for biomedical technology and technical medicine, University of Twente, Enschede, 7500 AE, The Netherlands

ARTICLE INFO

Keywords:

Pedunculopontine nucleus (PPN)
Basal ganglia-brain stem circuit
Deep brain stimulation (DBS)
Parkinson's disease (PD)

ABSTRACT

The pedunculopontine nucleus has been suggested as a target for DBS. In this paper we propose a single compartment computational model for a PPN Type I cell and compare its dynamic behavior with experimental data. The model shows bursts after a period of hyperpolarization and spontaneous firing at 8 Hz. Bifurcation analysis of the single PPN cell shows bistability of fast and slow spiking solutions for a range of applied currents. A network model for STN, GPe and GPi produces basal ganglia output that is used as input for the PPN cell. The conductances for projections from the STN and the GPi to the PPN are determined from experimental data. The resulting behavior of the PPN cell is studied under normal and Parkinsonian conditions of the basal ganglia network. The effect of high frequency stimulation of the STN is considered as well as the effect of combined high frequency stimulation of the STN and the PPN at various frequencies. The relay properties of the PPN cell demonstrate that the combined high frequency stimulation of STN and low frequency (10 Hz, 25 Hz, 40 Hz) stimulation of PPN hardly improves the effect of exclusive STN stimulation. Moreover, PPN-DBS at low stimulation amplitude has a better effect than at higher stimulation amplitude. The effect of PPN output on the basal ganglia is investigated, in particular the effect of STN-DBS and/or PPN-DBS on the pathological firing pattern of STN and GPe cells. PPN-DBS eliminates the pathological firing pattern of STN and GPe cells, whereas STN-DBS and combined STN-DBS and PPN-DBS eliminate the pathological firing pattern only from STN cells.

© 2011 Elsevier Ltd. All rights reserved.

1. Introduction

Parkinson's disease (PD) is a progressive, neurodegenerative disorder primarily associated with motor symptoms such as muscle rigidity, tremor of the limbs at rest, slowness and impaired scaling of voluntary movement (bradykinesia), loss of voluntary movements (akinesia) and postural instability (Jankovic, 2008). PD is characterized by the loss of dopaminergic cells in the substantia nigra pars compacta (SN_c). In early stages of PD, treatment with dopaminergic drugs can alleviate tremor, rigidity and bradykinesia. When medication is no longer effective, deep brain stimulation (DBS) can be applied to alleviate tremor and other Parkinson related symptoms successfully, if stimulation amplitude and frequency are properly chosen. In particular, high frequencies (130–185 Hz) are required. Currently, DBS for PD is widely applied in the subthalamic nucleus (STN), the globus pallidus pars interna (GPi) and the ventral intermediate thalamic nucleus.

For many patients STN/GPi-DBS is successful for cardinal symptoms, but has only limited effect for axial symptoms, such

as gait disturbances and postural instability. Stimulation of these targets mainly affects the thalamocortical output of the basal ganglia to cortical motor areas, whereas the axial muscles involved in locomotion and posture are mainly controlled from the brain stem (Nandi, Aziz, Liu, & Stein, 2002). These symptoms are particularly resistant to dopaminergic drugs. This suggests the involvement of non-dopaminergic pathways in the pathophysiology of these symptoms (Hamani, Stone, Laxton, & Lozano, 2007). Since the pedunculopontine nucleus (PPN) in the brain stem connects to nuclei in the basal ganglia and the spinal cord and its role in locomotion and postural control (Hamani et al., 2007; Pahapill & Lozano, 2000), this nucleus has been suggested as a target for DBS to improve gait and postural instability (Plaha & Gill, 2005).

The PPN is a rostral brain stem structure consisting of cholinergic and non-cholinergic neurons belonging to the ascending reticular activating system and the mesencephalic locomotor region (Mena-Segovia, Bolam, & Magill, 2004). The PPN can be subdivided into two parts based on neuron density and neurochemical characteristics: the pars compacta (PPN_c) and the pars dissipata (PPN_d) (Olszewski & Baxter, 1954). The PPN_c consists mainly of large cholinergic neurons (Jenkinson et al., 2009). The PPN_d consists of small and medium sized neurons with approximately the same number of cholinergic and non-cholinergic neurons (Hamani et al., 2007). Non-cholinergic PPN neurons

* Corresponding address: University of Twente, EWI-AAMP, PO Box 217, 7500AE, Enschede, The Netherlands. Tel.: +31 53 4893401.

E-mail addresses: M.A.J.Lourens@utwente.nl (M.A.J. Lourens), H.G.E.Meijer@utwente.nl (H.G.E. Meijer), T.Heida@utwente.nl (T. Heida), E.Marani@utwente.nl (E. Marani), S.A.vanGils@utwente.nl (S.A. van Gils).

are mostly glutamatergic, but also noradrenergic, dopaminergic, GABAergic (interneurons) and peptidergic (Pahapill & Lozano, 2000).

The main input from the basal ganglia to the PPN are the GABAergic projection from GPi and the substantia nigra pars compacta (SN_c), predominantly to the non-cholinergic neurons of the PPN_d (Pahapill & Lozano, 2000). The glutamatergic neurons of the PPN_d play an important role in the regulation of the basal ganglia and spinal cord (Pahapill & Lozano, 2000). The cholinergic PPN_c is a principal component in a feedback loop from the spinal cord and limbic system back into the basal ganglia and thalamus (Pahapill & Lozano, 2000).

Three types (I, II and III) of the PPN neurons have been characterized based on their intrinsic electrical membrane properties as obtained from intracellular recording (Kang & Kitai, 1990; Takakusaki & Kitai, 1997; Takakusaki, Shiroyama, & Kitai, 1997; Takakusaki, Shiroyama, Yamamoto, & Kitai, 1996). Type I neurons are characterized by low threshold calcium spikes (LTS), which give rise to a burst of fast action potentials after the offset of a hyperpolarizing current. The neurons also fire bursts of spikes when a depolarized stimulus is given during hyperpolarization. Type I neurons are non-cholinergic (Kang & Kitai, 1990) and probably glutamatergic (Takakusaki et al., 1996). Type II neurons do not burst, but instead they fire single action potentials with a large afterhyperpolarization in response to a depolarizing injected current. About 50% of type II neurons are cholinergic. Type III has neither the characteristics of both type I and type II.

In contrast to the high frequency stimulation of STN/GPi, stimulation of PPN should be applied with low frequency (20–25 Hz) to improve gait disturbances and postural instability (Mazzone et al., 2005; Plaha & Gill, 2005). For these symptoms low frequency stimulation of the PPN combined with standard DBS of the STN seems to be clinically more effective (Galati, Scarnati, Mazzone, Stanzione, & Stefani, 2008; Stefani et al., 2007). So the question arises why PPN should be stimulated at low frequencies. Despite real therapeutic successes, the fundamental physiological mechanisms underlying the effect of DBS are still not understood.

Pathophysiology of PD is characterized by increased firing rates of cells in the basal ganglia, a tendency toward bursting and abnormal synchronization in the cells of STN and GP (Brown, 2003). In particular, the synchronization at low frequencies (<30) are thought to be related to motor impairment in PD (Brown, 2003). A hypothesis is that high frequency stimulation of basal ganglia nuclei masks the pathological synchronized firing patterns of the basal ganglia with a regularized firing pattern. In the usual targets for high frequency stimulation in the basal ganglia, the neurons fire spontaneously at frequencies around 50 Hz and can easily follow the high frequencies of the stimulation. By following the high frequencies of the stimulation, the basal ganglia neurons are driving in a tonic mode, that prevents them relapsing into the pathological synchronized firing pattern. On the other hand, PPN neurons fire spontaneously at lower frequencies around 10 Hz and high frequency stimulation would probably silence rather than drive them. Androulidakis, Khan et al. (2008); Androulidakis, Mazzone et al. (2008) shows that when akinesia is successfully alleviated in PD by L-Dopa, this is associated with the return of a 10 Hz component in the correlation between the PPN and the sensorimotor cortex. It seems that low frequency stimulation will assist PPN to return to its natural 10 Hz oscillations, which in turn facilitates locomotion and postural control.

The aim of this paper is to investigate, with a computational model, how the PPN responds to physiological and pathological inputs of the basal ganglia. Moreover, we will investigate the effects of DBS in STN and PPN on the behavior of the network. To achieve this aim we first develop a computational conductance-based model for PPN, as such model is not yet available. We model

PPN type I neurons, because projections from the basal ganglia are primarily to the glutamatergic PPN neurons (type I) and these neurons provide the prominent descending PPN output to the spinal cord. Second, we generate basal ganglia input to the PPN type I model using the basal ganglia model as proposed by Rubin and Terman (2004). The model of Rubin and Terman (2004) has well defined physiological and pathological (Parkinsonian) states. To investigate the effect of STN-DBS and/or PPN-DBS we look at relay capability of the PPN cell to relay excitatory cortical input. Finally we make projections from the PPN back to the basal ganglia to investigate the effect of STN-DBS and/or PPN-DBS on the pathological firing pattern of STN and globus pallidus pars externa (GPe) cells.

2. Methods

2.1. PPN model

We have modeled the PPN type I neuron as a single compartment model. Based on the work of Takakusaki and Kitai (1997) we include in our model a persistent sodium current ($I_{Na,p}$) and T-type calcium current (I_T). The persistent sodium current is responsible for subthreshold membrane oscillations in PPN type I neurons, which underlies spontaneous repetitive firing. T-type calcium current is responsible for bursts of low threshold spikes. To produce action potentials in response to depolarizing current the model includes a sodium current (I_{Na}) and potassium current (I_K). The resting potential is defined by sodium ($I_{Na,L}$) and potassium ($I_{K,L}$) leak currents. In addition the model contains a hyperpolarization-activated current (I_{hyp}) to recover faster from hyperpolarization and facilitate the burst. The time-derivative of the membrane potential ($V_{m,PPN}$) of the PPN type I neuron is given by:

$$C \frac{dV_{m,PPN}}{dt} = -I_{Na,L} - I_{K,L} - I_{Na} - I_K - I_T - I_{hyp} - I_{Na,p} + I_{app}, \quad (1)$$

where C is the membrane capacitance, I_{app} is the applied current. The ionic currents are conductance-based and described according to the Hodgkin–Huxley formalism, except for the T-type calcium current which includes the Goldman–Hodgkin–Katz ion current equation (Appendix). The exact voltage dependence and kinetics of PPN ionic currents are based on similar neurons, namely the thalamocortical relay neuron (Destexhe, Neubig, Ulrich, & Huguenard, 1998; Huguenard & McCormick, 1992; McCormick & Huguenard, 1992) and the pre-Bötzinger neuron (Rybäk, Ptak, Shevtsova, & McCrimmon, 2003; Rybäk, Shevtsova, St-John, Paton, & Pierrefiche, 2003), as there are no reports in literature of such data for the PPN.

2.2. The network model

In order to investigate the effect of the basal ganglia input to the PPN cell, we have generated such input using the basal ganglia model as proposed by Rubin and Terman (2004). They modeled the indirect pathway of the basal ganglia that includes a population of STN, GPe, GPi and thalamic relay cells. In their model each STN, GPe and GPi cell is represented as a single compartment conductance-based model. Our network consist of 8 STN cells, 8 GPe cells, 8 GPi cells and 1 PPN cell and excludes the thalamic relay cells.

For the synaptic connections between the STN and GPe cells we use the structured sparsely connected architecture (Fig. 1), as in Terman, Rubin, Yew, and Wilson (2002). This network can reproduce both correlated rhythmic activity (clustered) and uncorrelated spiking. Each STN cell receives inhibitory input from two GPe cells. Each GPe cell receives excitatory input from one STN cell and inhibitory input from two immediate GPe neighbors. Each GPe cell also receives a constant current input representing striatal input. Each GPi cell receives excitatory input from one STN cell and inhibitory input from one GPe cell (Rubin & Terman, 2004). Finally, four STN cells and four GPi cells project excitatory (glutamatergic)

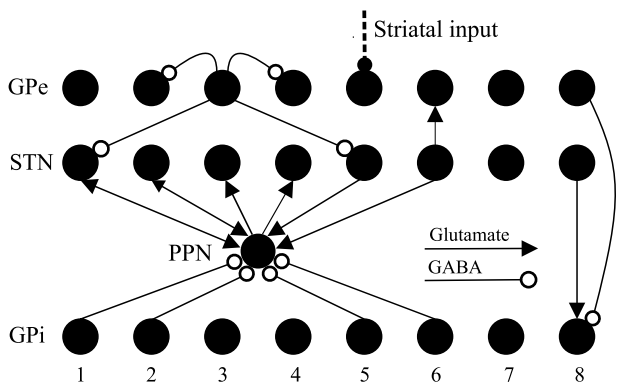


Fig. 1. The network architecture. For the STN–GPe connection the structured sparsely architecture from Terman et al. (2002) is adopted. GPe cell i inhibits its two immediate GPe neighbors ($i + 1$ and $i - 1$) as well as two STN cells ($i - 2$ and $i + 2$) by skipping the three STN cells located nearest to it. Here i runs from 1 to 8. In addition, GPe cells uniformly receive constant current inhibition from striatum. Each STN cell sends excitation to its nearest GPe cell (same index). Each GPi cell receives inhibition from the nearest GPe cell and excitation from the nearest STN cell. The PPN cell receives inhibition from GPi cell 1, 2, 5 and 6 and excitation from STN cell 1, 2, 5 and 6. In our PD simulations the STN cells 1, 2, 5 and 6 are active as a cluster. In our network of Section 2.6 the PPN cell sends also excitation to STN cell 1, 2, 3 and 4. The network architecture has a periodic structure. Lines ending with arrows and open circles indicate excitatory glutamatergic and inhibitory GABAergic synaptic connections, respectively.

respectively inhibitory (GABAergic) to the PPN cell, see Fig. 1. As in Rubin and Terman (2004) the synaptic current to the PPN is modeled as

$$I_{\alpha \rightarrow PPN} = g_{\alpha \rightarrow PPN}(V_{m,PPN} - E_{\alpha \rightarrow PPN}) \sum_j s_{\alpha}^j, \quad (2)$$

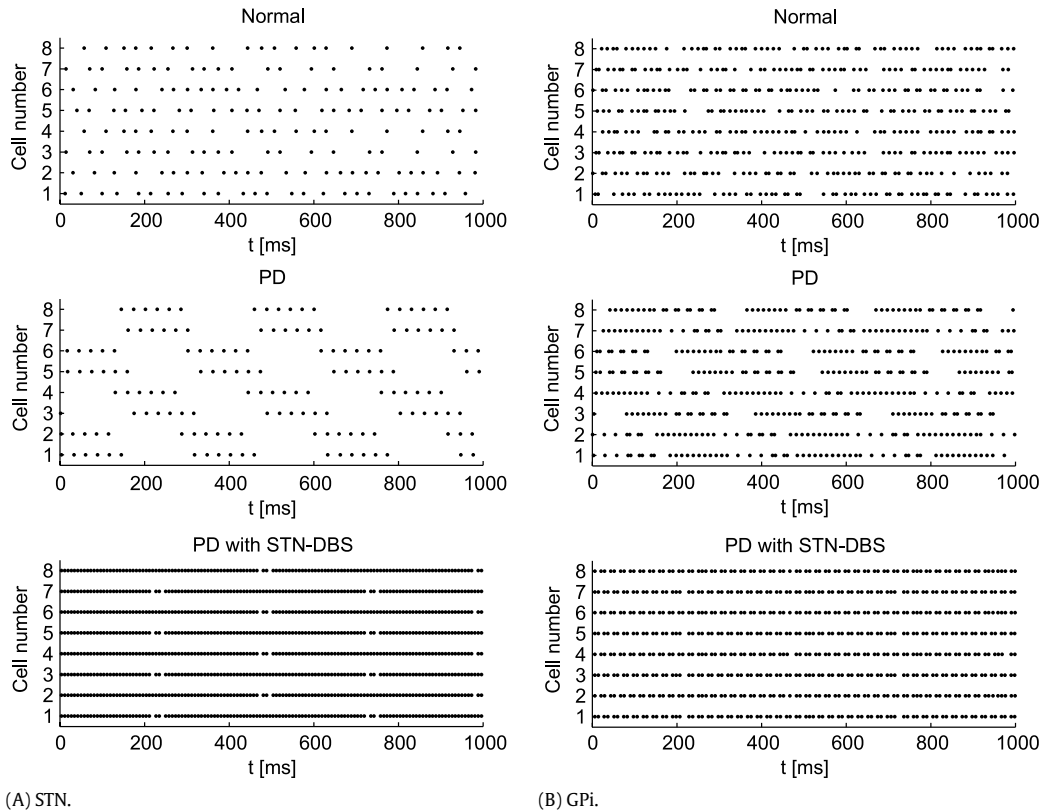


Fig. 2. Raster plots of the spike times for all eight STN cells (A) and all eight GPi cells (B) in the normal (top), PD (middle) and PD with STN–DBS (bottom) state. In the normal state the firing patterns of both types of cells are irregular and uncorrelated. In the PD state STN cells fire in a bursty and clustered pattern around 3 Hz and the cells within each cluster are almost synchronized (small lag). The GPi cells fire in a similar manner, but are less bursty. In the PD state with STN–DBS the STN cells are locked to the DBS frequency and GPi cells are partially locked by half the DBS frequency.

where $I_{\alpha \rightarrow PPN}$ is the synaptic current from structure α to the PPN cell, α is STN or GPi, $g_{\alpha \rightarrow PPN}$ is the maximal synaptic conductance and $E_{\alpha \rightarrow PPN}$ the reversal potential. For STN we take $g_{STN \rightarrow PPN} = 0.15 \text{ mS cm}^{-2}$ and $E_{STN \rightarrow PPN} = 0 \text{ mV}$, and for GPi we take $g_{GPi \rightarrow PPN} = 0.1 \text{ mS cm}^{-2}$ and $E_{GPi \rightarrow PPN} = -95 \text{ mV}$. The summation is taken over the STN/GPi cells that project to the PPN cell. Each synaptic variable s_{α}^j satisfies a first-order differential equation of the form:

$$\frac{ds_{\alpha}}{dt} = A_{\alpha}(1 - s_{\alpha})H_{\infty}(V_{m,\alpha} - \theta_{\alpha}) - B_{\alpha}s_{\alpha}, \quad (3)$$

where H_{∞} is a smooth approximation of the Heaviside step function. The kinetic parameters for STN and GPi are $[A_{\alpha}, B_{\alpha}, \theta_{\alpha}] = (1, 5, 30), (2, 0.1, 20)$, respectively.

2.3. Normal and parkinsonian states of the basal ganglia

Depending on the architecture and strengths of synaptic connections between the STN and GPe, within the GPe, and the striatal input to the STN–GPe network the model shows correlated rhythmic activity, uncorrelated spiking and propagating waves. It has been found in experiments that during PD there is an increased synchrony between nuclei in the basal ganglia while neurons fire in a bursty mode. As demonstrated in Terman et al. (2002), STN and GPe cells connected through a structured sparse architecture can fire irregularly with weak correlation between the cells as well as in clusters with high correlation between the cells. By using a structured sparse architecture we mimic a basal ganglia input to the PPN cell that represents a normal (uncorrelated spiking) or PD (correlated rhythmic activity) situation, see Fig. 2 (top and middle). Following the approach of Pirini, Rocchi, Sensi, and Chiari (2009) and Rubin and Terman (2004), only two parameters

are used to switch between the normal and the PD state: the indirect striatal current to GPe cells ($I_{\text{striatum} \rightarrow \text{GPe}}$) and the intra-GPe inhibitory synaptic conductance ($g_{\text{GPe} \rightarrow \text{GPe}}$). In the normal state we use $I_{\text{striatum} \rightarrow \text{GPe}} = 1.1 \mu\text{A cm}^{-2}$ and $g_{\text{GPe} \rightarrow \text{GPe}} = 1 \text{ mS cm}^{-2}$. In the PD state $I_{\text{striatum} \rightarrow \text{GPe}} = -3.5 \mu\text{A cm}^{-2}$ and $g_{\text{GPe} \rightarrow \text{GPe}} = 0.05 \text{ mS cm}^{-2}$. The increase in inhibitory striatal input to the GPe in PD is motivated by the fact that the activation of the D2-receptors in the striatum in PD is decreased, due to dopamine depletion in PD. This decreased activation leads to less inhibition of the striatal input to the GPe. Rubin and Terman (2004) motivated the decrease of the intra-GPe inhibitory synaptic conductance in PD on experimental results in rats (Ogura & Kita, 2000; Stanford & Cooper, 1999).

2.4. Deep brain stimulation

In our network model we apply DBS to STN and PPN. As in Rubin and Terman (2004) the effect of DBS on its target cells is modeled as a train of positive current pulses, injected directly into the target cells:

$$I_{\text{DBS}} = i_D H_\infty(\sin(2\pi f_{\text{DBS}} t))(1 - H_\infty(\sin(2\pi f_{\text{DBS}}(t + \delta_{\text{DBS}})))), \quad (4)$$

where H_∞ is a smooth approximation of the Heaviside step function, i_D is the amplitude of the injected current, f_{DBS} is the frequency of the DBS pulse train and δ_{DBS} is the duration of each impulse.

In the case of STN-DBS we assume that each STN cell receives the same DBS signal. STN-DBS is only applied in the PD state, with $i_D = 400 \mu\text{A cm}^{-2}$, $f_{\text{DBS}} = 130 \text{ Hz}$ and $\delta_{\text{DBS}} = 0.15 \text{ ms}$. Pirini et al. (2009) have demonstrated that these values for STN-DBS ensure a 1:1 ratio between DBS pulses and the action potentials of the STN cells (Fig. 2(A) (bottom)).

Our PPN cell receives DBS in the PD state of the network as well in the PD with STN-DBS state, as the combined stimulation seems to be clinically more effective (Galati et al., 2008; Stefani et al., 2007). The settings for PPN-DBS are $\delta_{\text{DBS}} = 0.15 \text{ ms}$, $f_{\text{DBS}} = 10\text{--}25\text{--}40 \text{ Hz}$ and $i_D = 10\text{--}100 \mu\text{A cm}^{-2}$. We use these frequencies as it was claimed that 25 Hz was optimal (Mazzone et al., 2005; Plaha & Gill, 2005).

2.5. Cortical input

In addition to input from the basal ganglia the PPN type I cell also receives excitatory cortical input (Jenkinson et al., 2009). To investigate the functionality of the PPN cell under normal, Parkinsonian, Parkinsonian with STN-DBS and/or PPN-DBS conditions, we test the relay capability of the PPN cell with excitatory, conductance-based, synaptic current $I_{\text{Cort.}}$:

$$I_{\text{Cort.}} = g_{\text{Cort.}} s(V_{m,\text{PPN}} - E_{\text{Glut.}}), \quad (5)$$

where s is the synaptic variable of the presynaptic cortex cell. The maximal conductance ($g_{\text{Cort.}}$) and the reversal potential ($E_{\text{Glut.}}$) are set to 0.15 mS cm^{-2} and 0 mV , respectively. At each spike of the cortex cell the synaptic variable is reset to 1, after which it decays exponentially with time constant $B_{\text{Cort.}}$:

$$\frac{ds}{dt} = -B_{\text{Cort.}} s. \quad (6)$$

$B_{\text{Cort.}}$ is set to 1 ms^{-1} . The spikes for the cortical input are selected from a Poisson distribution, with an enforced pause of 10 ms between spikes to avoid excessive firing. We use cortical Poisson inputs with mean rates of 12, 25 and 45 Hz.

2.6. PPN output to basal ganglia

The two key functions of the PPN is to relay and to regulate the basal ganglia activity (Mena-Segovia et al., 2004). In particular, the function of the PPN type I cell can be seen as regulator of the basal

ganglia (Pahapill & Lozano, 2000). These functions imply that the PPN and the basal ganglia are highly interconnected. To investigate the regulation function of the PPN type I under normal, Parkinsonian, Parkinsonian with STN-DBS and/or PPN-DBS conditions, we have also extended our model with PPN connections back to the basal ganglia. The major projections from the PPN to the basal ganglia are the projections to the STN and SN_c (Jenkinson et al., 2009). The PPN projections to STN are distributed uniformly throughout the STN (Jenkinson et al., 2009) and are cholinergic, glutamatergic and GABAergic (Mena-Segovia et al., 2004). We choose for a total of four glutamatergic projections by our PPN type I cell; two to adjacent STN cells, that connect to PPN, forming reciprocal connections, and two to adjacent STN cells, which are not connected to PPN (Fig. 1).

The synaptic current from PPN to STN cell j ($I_{\text{PPN} \rightarrow \text{STN},j}$) is modeled as

$$I_{\text{PPN} \rightarrow \text{STN},j} = g_{\text{PPN} \rightarrow \text{STN}}(V_{m,\text{STN},j} - E_{\text{PPN} \rightarrow \text{STN}})s_{\text{PPN}}, \quad (7)$$

where s_{PPN} is the synaptic variable of the PPN cell and $V_{m,\text{STN},j}$ the membrane potential of STN cell j . The maximal synaptic conductance ($g_{\text{PPN} \rightarrow \text{STN}}$) and the reversal potential $E_{\text{PPN} \rightarrow \text{STN}}$ are set to 0.15 mS cm^{-2} and 0 mV , respectively. The dynamics of the synaptic variable of the PPN cell is modeled with Eqs. (3) and use the same kinetic parameters as we used for the STN cell, namely $[A_\alpha, B_\alpha, \theta_\alpha] = (1, 5, 30)$.

We use the same parameters setting that we employed for the network without feedback to switch between a normal and PD behavior.

2.7. Simulation

The PPN type I model and the network model are implemented in MATLAB (Mathworks, Inc., Natick, MA, USA). To simulate the firing properties of the isolated PPN cell we use a stiff integrator (ODE15s in MATLAB) with maximum step size 0.1 ms and relative tolerance 10^{-6} . We exclude effects of initial transients by ignoring the first 400 ms of PPN cell simulations. The bifurcation analysis of the PPN cell is done within MATCONT, a bifurcation analysis tool (Dhooge, Govaerts, & Kuznetsov, 2003). For the network model without projections from PPN to STN the same numerical method is used except for the relative tolerance, which is now set to 10^{-4} for the integration of the STN-GPe-GPi network. For the simulation of the STN-GPe-GPi network we ignore the first 6 s before we use it as input to the PPN cell. For the simulations with PPN projections to the STN we used the fourth-order Adams Predictor-Corrector method with fixed step size of 0.01 ms to integrate the STN-GPe-GPi-PPN network. To speed up the calculation we have made a minor modification to the PPN model. The voltage depending time constants for the (in)activations gating variables of the persistent sodium channels are bounded from below by 0.01 ms. This modification does not effect the response of the PPN cell to depolarizing and hyperpolarizing stimuli. For these simulations we ignore the first 2 s.

Spectral analysis is done with MATLAB using Neurospec (<http://www.neurospec.org>) and is based on Halliday et al. (1995). Autospectra of the PPN spike times are calculated by dividing 10 s simulation data in 6 equal-length segments, providing a resolution of 0.6 Hz, and by averaging their Fourier transform. For additional smoothing of the autospectra we use a Hanning filter. The spike times are obtained from the voltage trace by a thresholding method (threshold is -20 mV).

To quantify the reliability and accuracy with which the PPN cell responds to the excitatory cortical inputs (Eq. (5)) we use the relay index (RI): The ratio of successfully relayed input and the total number of excitatory inputs. Specifically, for each excitatory cortical input, we record a successfully relayed input if at least

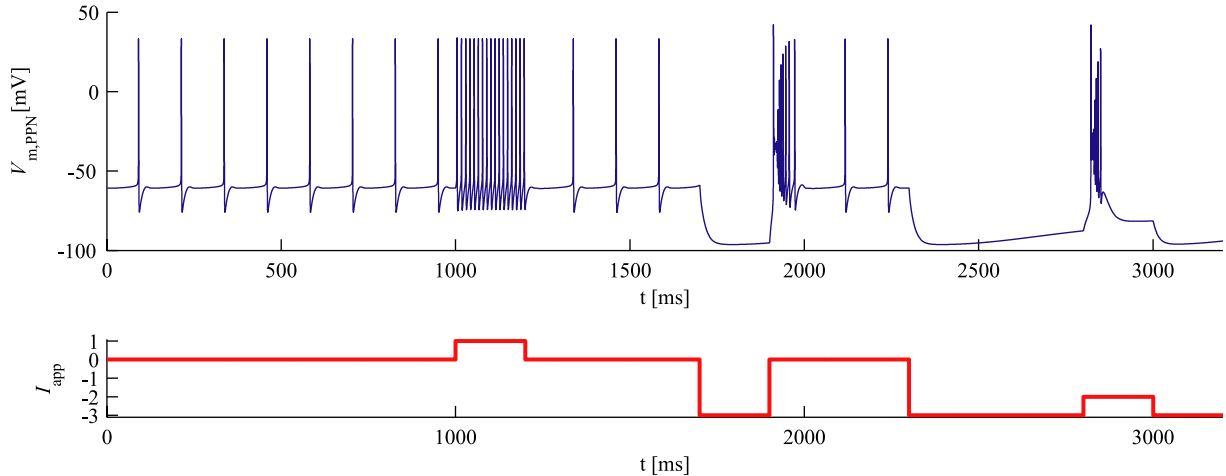


Fig. 3. Properties of the PPN model type I: first second spontaneous firing at approximately 8 Hz; after the first second response to a depolarizing stimulus; last 1.5 s response to a hyperpolarizing stimulus and depolarizing stimulus during hyperpolarization. Below the voltage trace the applied stimulus is shown (I [$\mu\text{A}/\text{cm}^2$]).

one PPN spike occurs within a window of 5 ms after the input arrives. Thus a RI of zero means no relay at all of the Poisson input, whereas a RI of one means a perfect relay. Each RI is averaged over 10 trials of 10 s simulation. The cortical Poisson input in each trial is different, but has the same mean rate.

3. Results

3.1. Firing properties of the isolated PPN neuron

The cell fires spontaneously at approximately 8 Hz (Fig. 3). The cell responds with high frequency spiking when a small depolarizing stimulus is given (Fig. 3). When the PPN cell is hyperpolarized, a burst appears at the end of the stimulus period or when a depolarizing stimulus is given during hyperpolarization (Fig. 3).

3.2. Bifurcation analysis of the isolated PPN neuron

Fig. 4 shows the bifurcation diagram of the PPN model with the applied current (I_{app}) as parameter. As the applied current increases the stable equilibrium (rest state) becomes unstable via a subcritical Hopf bifurcation (H_1), with unstable limit cycles bifurcating. The equilibrium is unstable until the second Hopf bifurcation (H_2). This Hopf bifurcation is supercritical, which means that stable limit cycles emerge. A stable limit cycle corresponds to continuous spiking.

Continuation of the limit cycle starting from H_2 shows a decrease in frequency as the applied current decreases. The limit cycle becomes unstable via a limit point bifurcation of limit cycles (Fig. 5, LPC_1). Continuing the limit cycle further it regains stability through a period doubling bifurcation (Fig. 5). The period then is nearly constant around 100 ms. This low frequency spiking limit cycle corresponds to the spontaneous firing of the PPN.

Both tonic spiking regimes have a type II phase response curve (Fig. 6), meaning that a perturbation of the limit cycle can produce a phase advance or phase delay depending on the timing. The phase shift of both the low and high frequency spiking solution becomes larger upon increasing, respectively decreasing, I_{app} towards the bifurcation points where they lose stability.

3.3. PPN with basal ganglia input

3.3.1. Normal

Fig. 7 shows the mean frequency of the PPN cell with normal input for different choices for the strength of the synaptic conductances from STN and Gpi to PPN. The mean frequency is

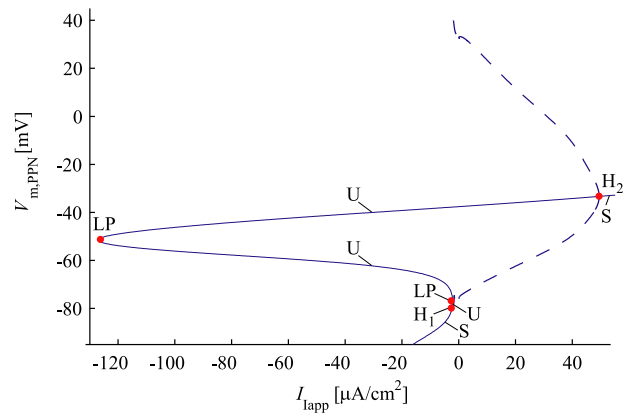


Fig. 4. Bifurcation analysis of the PPN model with I_{app} as free parameter. Solid curve shows the equilibrium value of the membrane potential ($V_{m,\text{PPN}}$). Labels S and U denote stable and unstable branches respectively. H_1 is a subcritical Hopf bifurcation, H_2 is a supercritical Hopf bifurcation and LP is a limit point bifurcation. Dashed curve shows the min/max value of the stable limit cycle.

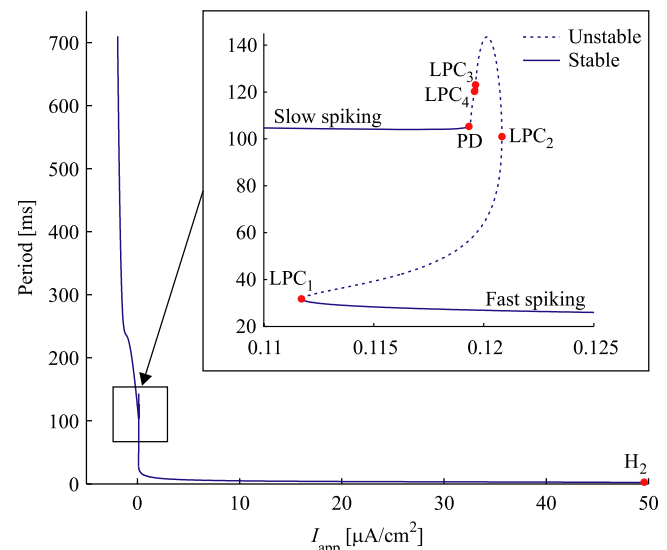


Fig. 5. Partial information about dynamical behavior: period of the spiking solutions as function of I_{app} . LPC is a limit point bifurcation of limit cycles and PD is a period doubling bifurcation.

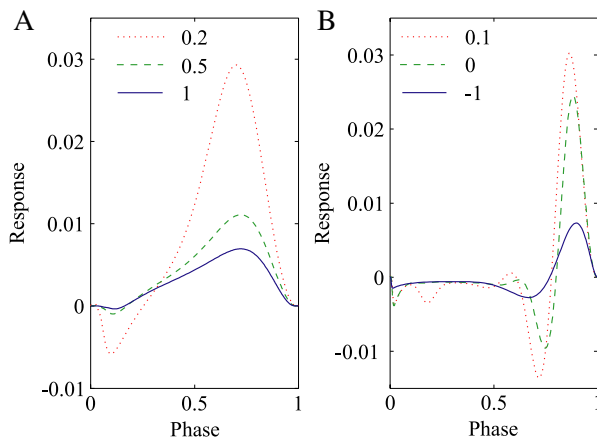


Fig. 6. PRCs of limit cycles in the PPN model, at different parameter values I_{app} [$\mu\text{A cm}^{-2}$]: (A) high frequency spiking; (B) low frequency spiking.

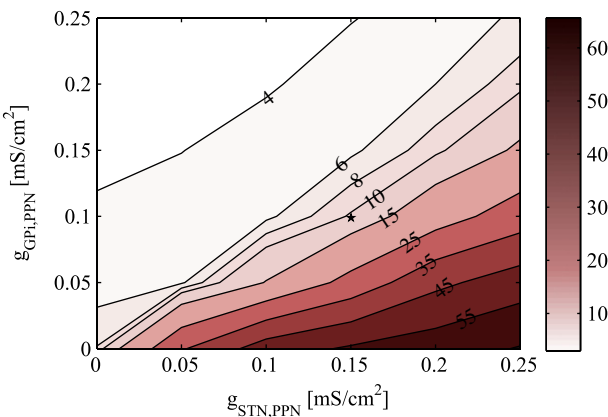


Fig. 7. Contour plot of the mean frequency of the PPN in the normal state for different choices for $g_{GPI \rightarrow PPN}$ and $g_{STN \rightarrow PPN}$. See text for details about calculation of the mean frequency. The marker \star indicates the values for the chosen parameters.

calculated from the reciprocal of the mean interspike interval over a period of 10 s. This figure was almost equal to the average number of spikes per second indicating that the response was not very bursty. We simulate a STN lesion in our model by setting the STN conductance to zero and adjust the GPI conductance to get a firing rate according to experiments of Breit, Bouali-Benazzouz, Benabid, and Benazzouz (2001) (2.9–6.6 Hz). Having the GPI conductance we then adjust the STN conductance to obtain a firing rate of the PPN cell under normal conditions. Experiments in anesthetized rat (Scarnati, Proia, Loreto, & Pacitti, 1987), and in monkeys (Matsumura, Watanabe, & Ohye, 1997) show that the majority of the PPN cells with a narrow spike width have an irregular firing pattern and a discharge rate of 10–20 Hz during spontaneous activity. It is proposed that the narrow spike width PPN cells are non-cholinergic and probably correspond to type I cells (Takakusaki & Kitai, 1997). This procedure yields a 10 Hz irregular firing rate for the normal input when we set $g_{GPI \rightarrow PPN} = 0.1 \text{ mS cm}^{-2}$ and $g_{STN \rightarrow PPN} = 0.15 \text{ mS cm}^{-2}$, see Fig. 7. We will not change these settings between the normal and PD states.

Fig. 8(A) (top) shows the total synaptic input from STN and GPI to the PPN cell during the normal state. In the normal state, the STN and GPI cells fire irregularly and uncorrelated (Fig. 2) leading to an irregular total synaptic input of the four STN and GPI cells projecting to PPN. The PPN cell fires with a mean frequency of 10.3 Hz which is slightly faster than its spontaneous behavior (Fig. 8(A) (middle)). In the autospectrum there is no clear peak

above the confidence level (Fig. 8(A) (bottom)). We conclude that the PPN cell fires in an irregular manner in response to irregular (Normal) input.

3.3.2. PD

The STN cells fire in a bursty and clustered pattern in the PD state (Fig. 2(A)). One cluster projects to the PPN cell resulting in excitation from STN in this bursting pattern around 3 Hz. The GPI cells behave similarly but fire less bursty (Fig. 2(B)) resulting in flatter level of inhibition, see Fig. 8(B) (top). The inhibitory input of GPI is relatively high compared to the excitatory input of STN, preventing the PPN from firing. At the onset of the STN clustered input the excitation to PPN becomes sufficiently high to overcome the inhibition of GPI, allowing the PPN to fire. In response to this increased excitation of the STN the inhibitory input of GPI increases, preventing the PPN cell to fire with the burst frequency of the STN input. The PPN cell responds with subthreshold oscillations during the STN clustered input. This regular input of STN and GPI resulting in a regular firing pattern of the PPN cell with a mean frequency of 3.19 Hz (Fig. 8(B) (middle)). This regularity is also reflected in the autospectrum of the PPN output. Clear peaks occur at the mean frequency and its superharmonics 6.4, 9.6, 12.8 Hz, etc. (Fig. 8(B) (bottom)).

3.3.3. PD with STN-DBS

Applying STN-DBS in the PD state, the bursting element in the STN input disappears and the STN input becomes tonic (130 Hz, DBS frequency) (Fig. 8(C) (top)). Also the GPI inhibition becomes more tonic. As a result the level of excitation to PPN is higher and the mean firing rate increases to 36.4 Hz (Fig. 8(C) (middle)). The autospectrum has a clear peak at the STN-DBS frequency and its subharmonics 86.7 and 43.3 Hz, but no clear peak at the PPN mean frequency (Fig. 8(C) (bottom)). Thus, STN-DBS makes the regular firing pattern of the PPN cell in PD more irregular, and introduces components of its frequency in the PPN output.

3.4. Effect of PPN-DBS

Fig. 9 shows the response of the PPN cell to PPN-DBS with amplitude of 100 $\mu\text{A cm}^{-2}$ and frequencies of 10, 25 and 40 Hz. In the PD state and without STN stimulation, the PPN cell is locked to its own stimulation frequency. This can be seen from the peaks in the autospectra at the PPN-DBS frequency and its subharmonics (Fig. 9(A)). At the higher frequencies (25 and 40 Hz) this locking is perfect, meaning the PPN cell fires with its own stimulation frequency. When STN-DBS is applied in the PD state and the PPN cell is stimulated, the locking of the PPN cell to its own stimulation frequency is less prominent, as seen in Fig. 9(B). STN-DBS disturbs the total synchronization between the PPN cell and its own stimulation. This effect of STN-DBS is less if the PPN-DBS frequency increases. This can be seen from the peaks at the STN-DBS frequency and its subharmonics in the autospectra of 10 and 25 Hz PPN stimulation, whereas the autospectrum of 40 Hz PPN stimulation has no clear peaks at the STN-DBS frequency.

Fig. 10 shows again the effect of PPN-DBS, but now with a lower stimulation amplitude of 10 $\mu\text{A cm}^{-2}$. In both network states (PD and PD with STN-DBS) and for all stimulation frequencies, the PPN-DBS is too weak to lock the PPN firing to the stimulus frequency. The regular 3 Hz firing of the PPN cell in the PD state disappears as the PPN-DBS frequency increases and becomes more irregular (peaks at 3 Hz and superharmonics disappear). The effect of STN-DBS is compared to the weak PPN-DBS strong and dominates the firing behavior of the PPN cell.

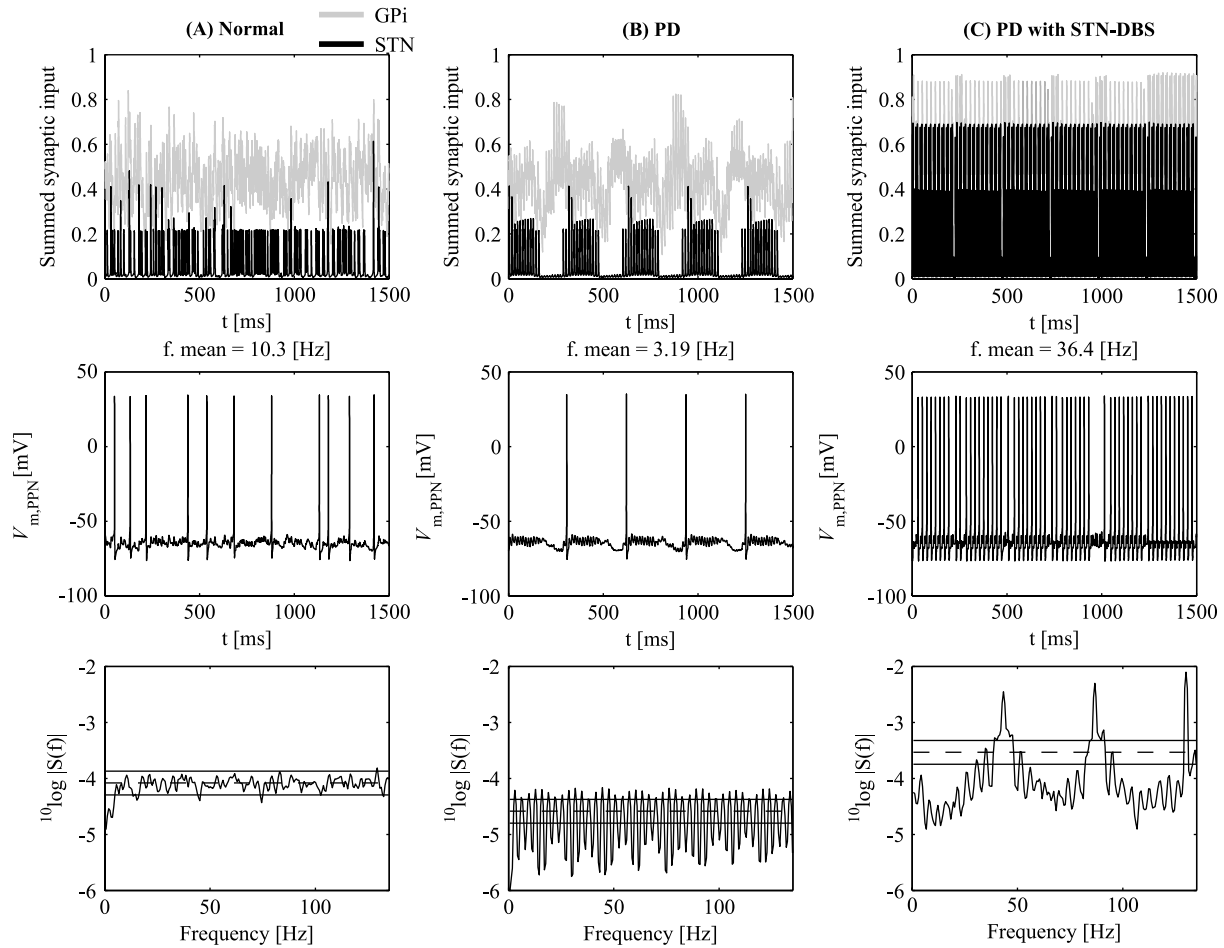


Fig. 8. Response of the PPN cell to inputs from the STN and GPi under normal (A), PD (B) and PD with STN-DBS conditions. Top: total synaptic input from GPi and STN received by the PPN cell under the different conditions. The synaptic input of GPi is defined as the normalized sum of the synaptic variables over the four GPi cells projecting to the PPN cell. Same definition holds for the STN input. Middle: voltage trace of the PPN cell. Bottom: autospectrum of the PPN spike times; see Section 2.7 for computational details.

Table 1

The Relay index (RI) of the PPN cell for the different situation in response to a cortical Poisson input to the PPN cell with mean frequency of 12, 25 and 45 Hz and conductance of 0.15 mS cm^{-2} . For STN-DBS the DBS settings are $i_{D,STN} = 400 \mu\text{A cm}^{-2}$, $f_{DBS,STN} = 130 \text{ Hz}$ and $\delta_{DBS,STN} = 0.15 \text{ ms}$ and for PPN-DBS the pulse width is $\delta_{DBS,PPN} = 0.15 \text{ ms}$.

State	Mean frequency of the cortical Poisson input					
	12 Hz		25 Hz		45 Hz	
Normal	0.75		0.71		0.65	
PD	0.75		0.71		0.64	
PD with STN-DBS	0.70		0.74		0.76	
	$i_{D,PPN} = 100$	$i_{D,PPN} = 10$	$i_{D,PPN} = 100$	$i_{D,PPN} = 10$	$i_{D,PPN} = 100$	$i_{D,PPN} = 10$
PD with PPN-DBS of 10 Hz	0.66	0.75	0.65	0.71	0.60	0.65
PD with PPN-DBS of 25 Hz	0.57	0.75	0.59	0.72	0.57	0.66
PD with PPN-DBS of 40 Hz	0.54	0.77	0.54	0.73	0.55	0.67
PD with STN and PPN-DBS of 10 Hz	0.71	0.70	0.72	0.74	0.74	0.77
PD with STN and PPN-DBS of 25 Hz	0.67	0.69	0.72	0.73	0.71	0.77
PD with STN and PPN-DBS of 40 Hz	0.66	0.69	0.67	0.73	0.68	0.78

3.5. Relay function of the PPN cell

Table 1 shows the relay index (RI) of the PPN cell for the different situations and for three mean rates of the Poisson trains. The RI in the normal state for the three different forms of input is almost the same as in the PD state: except for the Poisson trains with mean rate 45 Hz the normal state is slightly better than the PD state. Compared to the normal and the PD state, STN-DBS improves the relay function of the PPN cell for the Poisson trains with mean rates 25 and 45 Hz. The relay functionality during high frequency STN-DBS simulation is almost never higher

with additional PPN-DBS stimulation. When PPN-DBS is applied, a lower amplitude ($10 \mu\text{A cm}^{-2}$) and higher frequency (40 Hz) shows better results than a higher amplitude ($100 \mu\text{A cm}^{-2}$) and lower frequencies (10 and 25 Hz).

3.6. The closed loop network

3.6.1. Normal, PD and PD with STN-DBS

In Section 3.3 we considered the output of the PPN receiving input of the basal ganglia in three different states. In this section

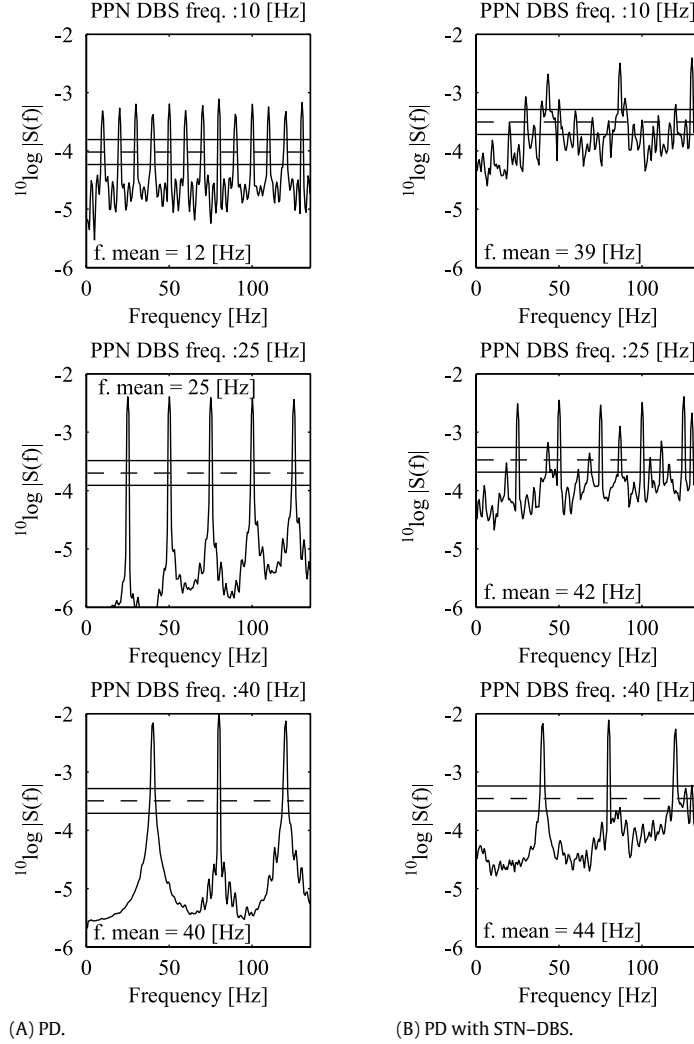


Fig. 9. Autospectrum of the PPN spike times with PPN-DBS applied. The PPN-DBS settings are $\delta_{\text{DBS}} = 0.15 \text{ ms}$, $f_{\text{DBS}} = 10\text{--}25\text{--}40 \text{ Hz}$ and $i_{\text{D}} = 100 \mu\text{A cm}^{-2}$. f. mean is the mean firing frequency of the PPN cell.

we consider again the three different states of the basal ganglia, but now we include feedback of the PPN type I cell to the STN cells as described in Section 2.6, to form the closed loop network.

Similarly as for the network without connections from the PPN to STN we examine how the mean frequency of the PPN cell with normal input changes as function of the synaptic conductances $g_{\text{GPI} \rightarrow \text{PPN}}$ and $g_{\text{STN} \rightarrow \text{PPN}}$, see Fig. 11. The result closely resembles the result of the network without feedback of PPN to STN (Fig. 7). We conclude that the feedback of PPN to STN has a minor effect on the mean frequency of the PPN under normal input conditions. For the other simulations we use $g_{\text{GPI} \rightarrow \text{PPN}} = 0.1 \text{ mS cm}^{-2}$ and $g_{\text{STN} \rightarrow \text{PPN}} = 0.15 \text{ mS cm}^{-2}$.

Fig. 12 (top) shows the total synaptic input from STN and GPI to the PPN cell in the three different basal ganglia states. The total synaptic input in all three states is very similar to the case when there is no feedback of PPN to STN. We observe that the firing pattern of the basal ganglia cells in the normal and PD state is not altered by our adding projections from the PPN to STN. Moreover, the PPN cell responds to these synaptic inputs in a similar manner as without the PPN to STN connections (Fig. 12 (middle and bottom)). The PPN cell fires irregular in the normal state with a mean frequency of 8.7 Hz. In the PD state, the firing pattern is regular and the mean frequency is decreased to 3.39 Hz. STN-DBS makes the regular firing pattern of the PPN cell in PD more irregular, and introduces components of its frequency in the PPN output.

3.6.2. Effects of PPN and STN-DBS in the closed loop network

Fig. 13 shows the effect of PPN-DBS stimulation (no STN-DBS) with low and high stimulation amplitude on STN and PPN activity. Initially, without external stimulation (until 1 s), the STN cells fire in a bursty and clustered pattern, which characterize the PD state. The PPN cell fires regularly around 3 Hz. When PPN-DBS is switched on, indicated by the arrow at 1 s, low amplitude ($10 \mu\text{A cm}^{-2}$) stimulation changes the firing pattern of the PPN cell from regular to irregular while doubling its mean firing rate to 6 Hz. This low amplitude stimulation of the PPN influences the activity of the STN clusters only episodically. In contrast, at high stimulation amplitude, the PPN activity is immediately overwritten by the stimulation, i.e. firing becomes locked to the stimulus. In turn some of the STN cells start firing regularly at a rate around 20 Hz. For low stimulus frequencies some clustering and bursting remains.

Next STN-DBS is turned on as well. We observe that the PPN activity becomes similar as described in Section 3.4 (Figs. 9(B) and 10(B)) and STN cells are locked to the STN-DBS.

STN-DBS does not interrupt the GPe bursty clustered firing patterns, also not when combined with PPN-DBS (Fig. 14(A)). PPN-DBS alone does disrupt this pattern and eliminates this activity from the entire network (Fig. 14(B)). The GPe cells start firing regularly at a rate around 20 Hz, like the STN cells do (Fig. 13). Switching on STN-DBS reintroduces the clusters in GPe activity (not shown). Finally we stress that in all simulations we see that

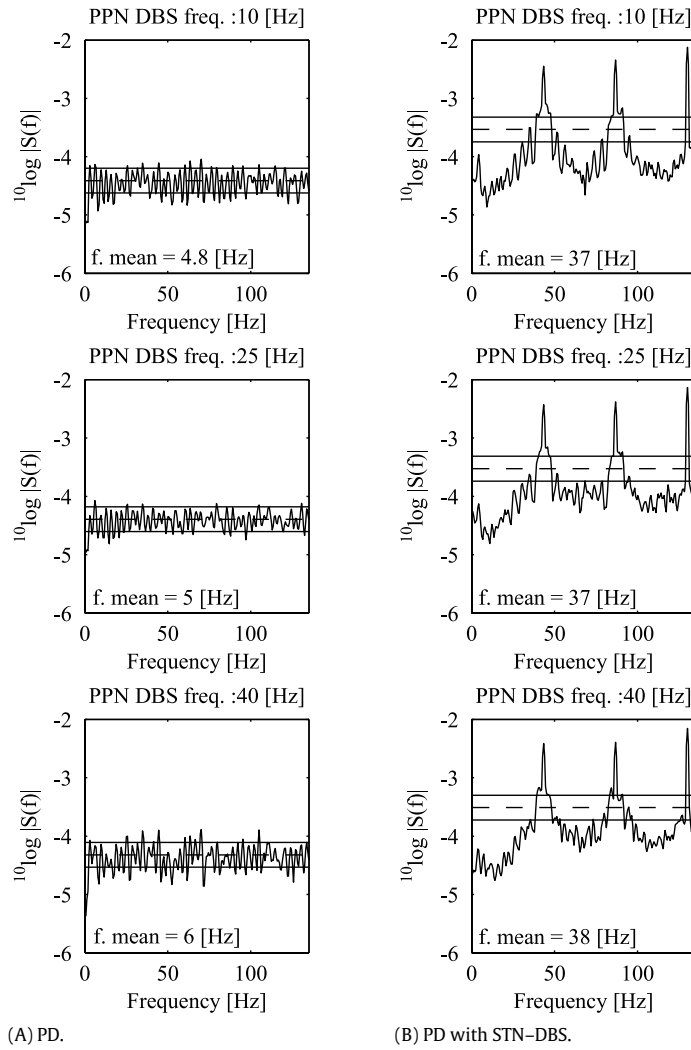


Fig. 10. Autospectrum of the PPN spike times with PPN-DBS applied. The PPN-DBS settings are $\delta_{\text{DBS}} = 0.15 \text{ ms}$, $f_{\text{DBS}} = 10\text{--}25\text{--}40 \text{ Hz}$ and $i_{\text{D}} = 10 \mu\text{A cm}^{-2}$. f. mean is the mean firing frequency of the PPN cell.

effects of PPN-DBS in the GPe and STN cells appears after several seconds.

4. Discussion

This study investigates the response of a single PPN type I cell to various inputs of the basal ganglia representing physiological, pathological and therapeutic cases. In particular, we look at the PPN spike output, that modulate the basal ganglia, and the relay of excitatory inputs as these are the key functions of the PPN cells (Mena-Segovia et al., 2004).

First, we have developed a computational model for a PPN type I cell and tuned it such that it reproduced known firing patterns (Takakusaki & Kitai, 1997): bursts after a period of hyperpolarization and spontaneous firing at 8 Hz (Fig. 3). The model shows that switching between low and high frequency spiking is possible. Bifurcation analysis confirms this and reveals that there is a bistability between high and low frequency tonic spiking (Fig. 5). For increasing current our PPN model shows an increasing frequency with a maximum of 450 Hz at $I_{\text{app}} = 50 \mu\text{A cm}^{-2}$, where the periodic orbit disappears through a Hopf bifurcation (Fig. 5). For higher currents the PPN cell is silent due to a depolarization blockade. Recently, Simon et al. (2010) did whole patch clamp recordings on rat brain stem slices and found that PPN cells have a gamma frequency (40–60 Hz) plateau when they are

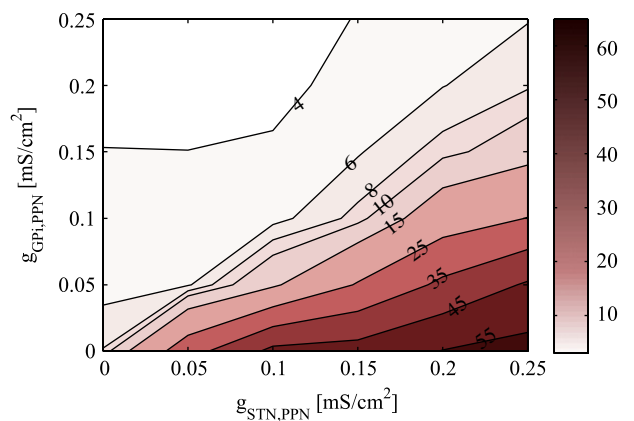


Fig. 11. Contour plot of the mean frequency of the PPN for different choices for $g_{\text{GPe} \rightarrow \text{PPN}}$ and $g_{\text{STN} \rightarrow \text{PPN}}$. The PPN receives normal input and sends excitatory input to the STN cells. The synaptic conductance from PPN to STN is constant and set to 0.15 mS cm^{-2} .

depolarized with increasing current steps. This behavior was not significantly different among the three PPN cell types, except that PPN type I cells fire faster than PPN type II or PPN type III cells during the beginning of the current injection. Simon et al. (2010) did not show hyperpolarization steps. In addition they did not

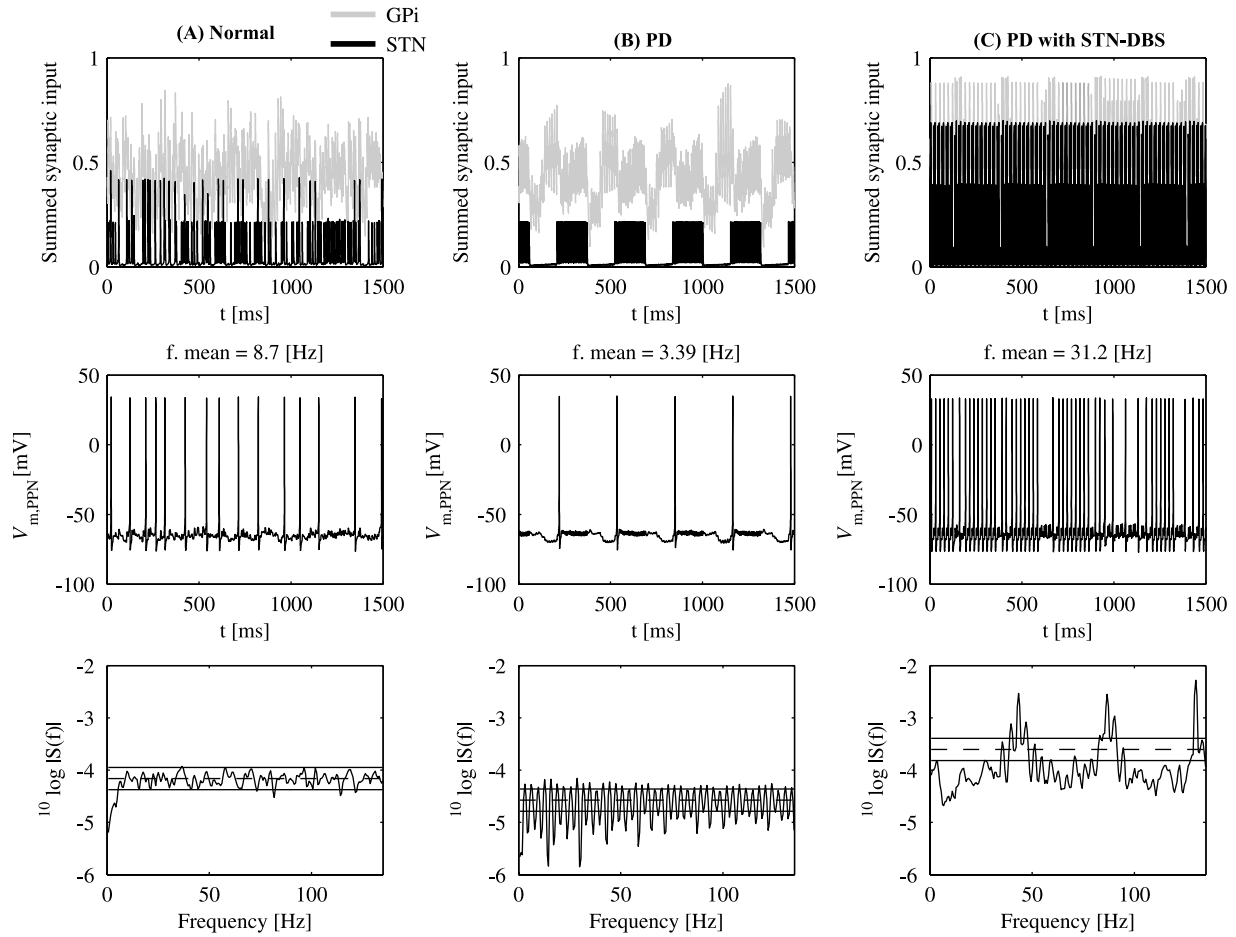


Fig. 12. Response of the PPN cell to inputs from the STN and GPi under normal (A), PD (B) and PD with STN-DBS conditions. The PPN cell sends also projections back to the STN; see Section 2.6. *Top:* total synaptic input from GPi and STN received by the PPN cell under the different conditions. The synaptic input of GPi is defined as the normalized sum of the synaptic variables over the four GPi cells projecting to the PPN cell. Same definition holds for the STN input. *Middle:* voltage trace of the PPN cell. *Bottom:* autospectrum of the PPN spike times; see Section 2.7 for computational details.

observe an abrupt switch between high and low frequency spiking as the applied current increases. In the low frequency range where we operate this discrepancy can be neglected.

The PPN is an output structure to many brain structures and receives modulatory input from the basal ganglia. We generated such basal ganglia input for three scenarios (Normal, PD and PD with STN-DBS) using an existing computational model of the STN-GPe-GPi subnetwork (Rubin & Terman, 2004). The response of the PPN model depends on the balance between the excitatory input from STN and inhibitory input from GPi, see Figs. 7 and 11. In general, the firing pattern of the PPN cell is more irregular for normal input, while the rate decreases and the pattern regularizes under PD conditions.

Experimental results are not conclusive about the balance between excitatory and inhibitory inputs to PPN and our simulations depend critically on this balance. On the one hand, Nandi, Aziz, Giladi, Winter, and Stein (2002) have shown that injection of a GABA antagonist into the PPN of MPTP treated primates markedly attenuates akinesia. This result suggests that in PD the neuronal activity of the PPN is suppressed by an excess of inhibition from GPi and SN_r leading to the hypoactivity symptoms. On the other hand, Breit et al. (2001) shows that in anesthetized dopamine depleted rats PPN cells fire more irregularly and in bursts with an increased firing rate as compared to controls (18–20 vs. 10–11 Hz). After lesion of the overactive STN in PD, the activity of the PPN is diminished, suggesting that the PPN is under major control of the STN.

In our model STN-DBS can modulate the activity of the PPN cell via a direct projection and via an indirect pathway via GPi. Florio et al. (2007) found that in normal and dopamine depleted rats approximately 40% of the recorded PPN neurons respond to STN-DBS, resulting from an unbalance between the excitatory and inhibitory pathways. Our simulations with and without PPN feedback to the STN show an increased mean firing rate of the PPN if STN-DBS is applied. This suggests that the PPN cell receives more direct than indirect STN-DBS input. As a result the PPN cell locks to the STN-DBS input, but does not fire on every cycle. On the contrary, Florio et al. (2007) found that approximately 85% of the responding PPN neurons responded to STN-DBS with inhibition, suggesting that the STN-DBS influence via the indirect inhibitory inputs are stronger. Moreover, they found that the balance between excitatory and inhibitory effects of the STN-DBS is independent from the dopaminergic nigral neurons. The balance is disturbed in rats with entopeduncular (rodents equivalent of GPi) lesion. In that case 75% of the PPN neurons become responsive to STN-DBS and are mostly (85%) excited by the STN-DBS.

A first report on PPN stimulation in human has shown that low frequency (20–25 Hz) stimulation of the pedunculopontine nucleus have acute improvement in motor function, such as gait and postural stability (Plaha & Gill, 2005). For frequencies higher than 30 Hz, the improvement in motor scores was variable, while very high frequencies (>180) worsened motor scores. Stefani et al. (2007) studied at combined stimulation of the PPN and STN. Their key finding was that PPN-DBS with medication was inferior to

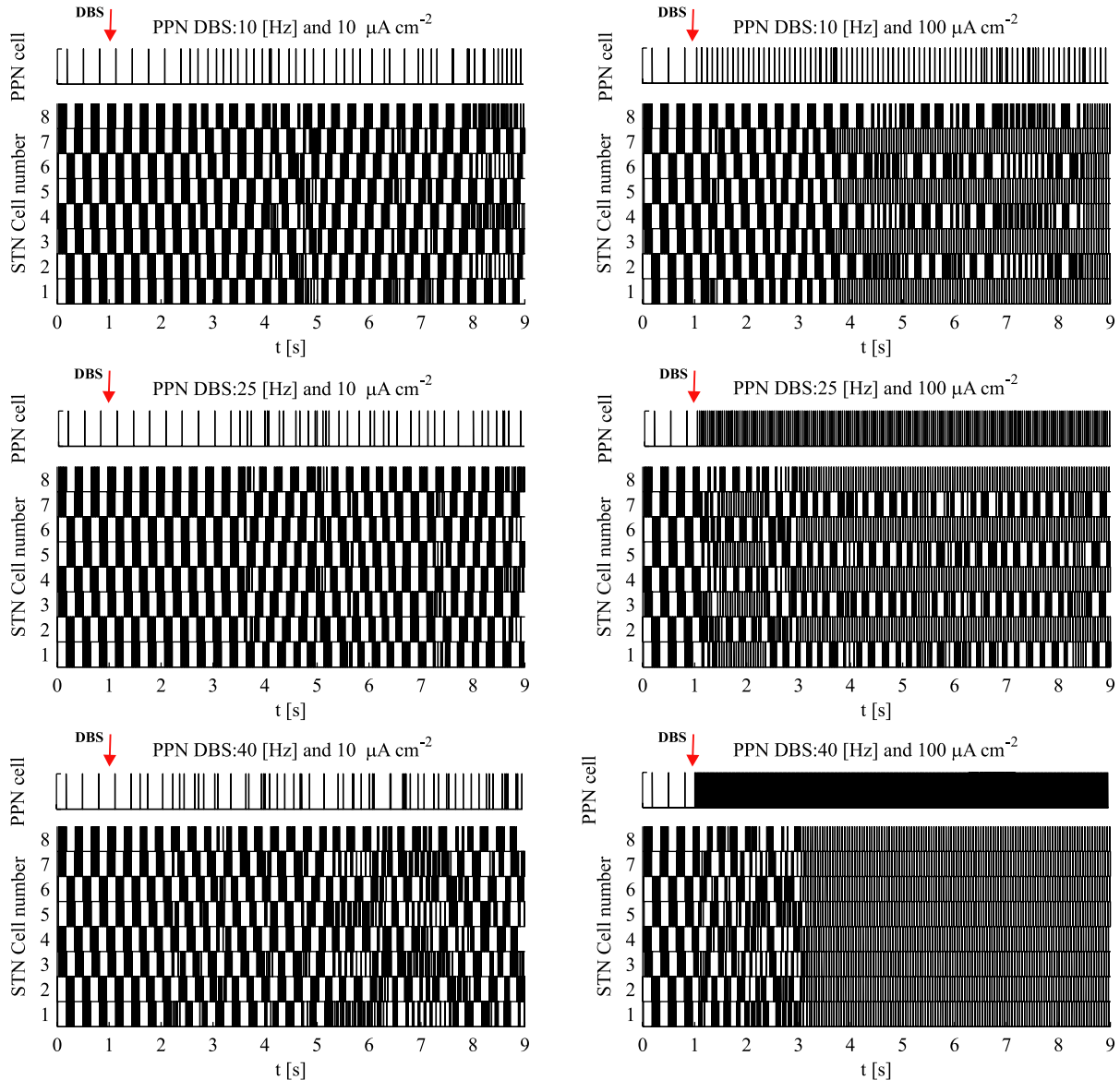


Fig. 13. Response of the STN cells in PD to different PPN-DBS settings. For each PPN-DBS setting the spike trains of all eight STN cells and the PPN cell are shown. The arrow above the PPN spike trains at 1 s indicates when PPN-DBS is switched on. The pulse width for all settings is 0.15 ms.

medication only, while it improved motor scores in combination with medication and STN-DBS as compared to medication and STN-DBS only. These results were obtained after 6 months. Another clinical validation of PPN-DBS did not show significant improvements in combination with or without medication and with or without STN-DBS, after 1 year (Ferraye et al., 2010). One may conclude that results of PPN-DBS vary from case to case.

To investigate the effect of STN-DBS and/or PPN-DBS in the network without projections from PPN to STN, we look at relay properties of the PPN cell (relay index). For the relay properties of the PPN cell it turns out that combined high frequency stimulation of the STN and PPN stimulation at low frequencies (10 Hz, 25 Hz, 40 Hz) is almost never better than exclusive STN stimulation. There are some doubts about the validity of the relay index. In the first place the main function of PPN type I cells is to regulate the basal ganglia activity. No improvement in the relay capability does not imply that PPN-DBS will not improve the basal ganglia activity. Second, the way we define the relay index. We record a successfully relayed excitatory cortical input if at least one PPN spike occurs in a specific time window after the input. As the PPN cell has a

spontaneous activity, the spike can be the result of the cortical input or the result of its own spontaneous activity.

We also investigate the effect of STN-DBS and/or PPN-DBS on the pathological firing pattern of STN and GPe. For this purpose we extended our network with feedback projection from PPN to STN. Our main finding is that high amplitude ($100 \mu\text{A cm}^{-2}$) PPN-DBS alone eliminates the pathological bursty clustered firing pattern from the STN and GPe cells and replaces it with regular firing pattern around 20 Hz. This 20 Hz is independent from the stimulus frequency, but for the low frequencies (10 and 25 Hz) some clustering and bursting remain. In contrast STN-DBS and combined STN-DBS and PPN-DBS eliminate the pathological firing pattern only from the STN cells and lock the STN activity to the STN-DBS. We conclude that PPN-DBS alone is the best way to eliminate the clusters and thereby the low frequency (3 Hz, associated with tremor) oscillations from the entire model network. However PPN-DBS creates a 20 Hz oscillation in the STN and GPe cells, which could also be pathological. Bradykinesia is associated with maintained oscillations in the β band in the STN (Kühn et al., 2008).

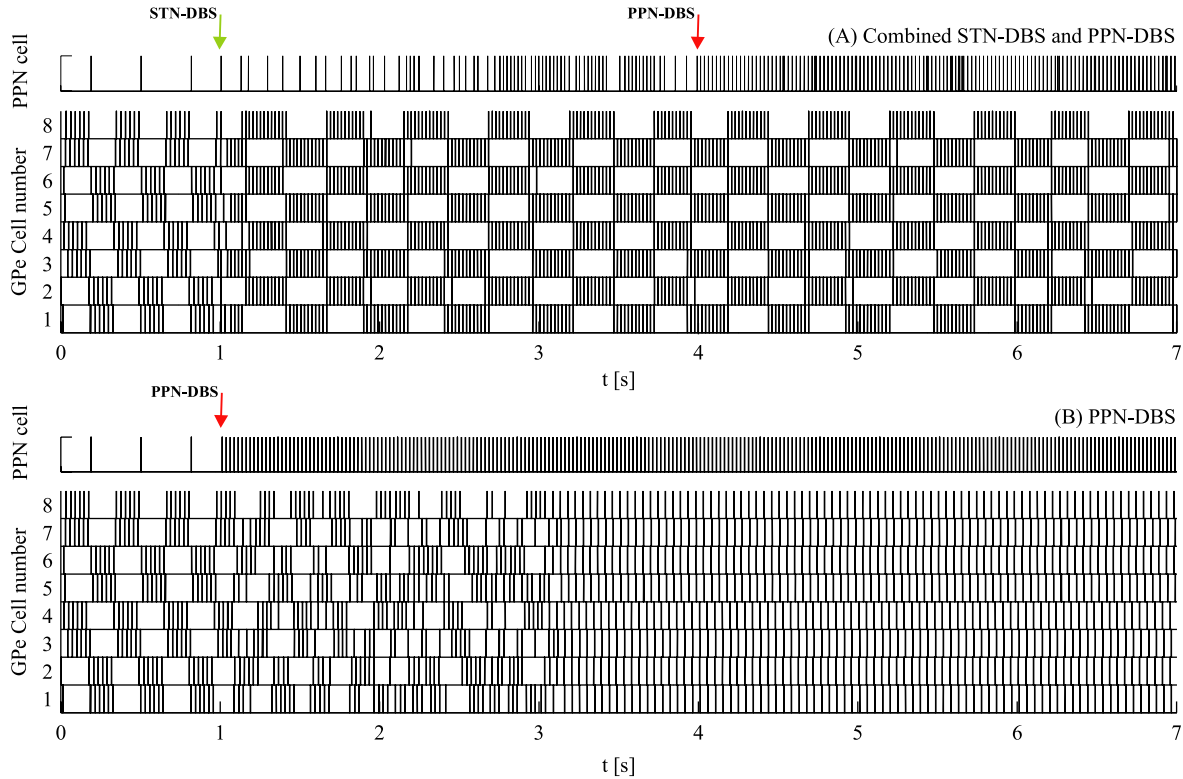


Fig. 14. Effect of PPN-DBS and STN-DBS on the activity of GPe cells. PPN-DBS is applied with high amplitude ($100 \mu\text{A cm}^{-2}$) at 40 Hz and STN-DBS is applied at 130 Hz with amplitude of $400 \mu\text{A cm}^{-2}$. For both stimulus a pulse width of 0.15 ms is used. Stimulation start at 1 and 4 s indicated by the arrow. With STN-DBS stimulation clusters remain and longer in duration. Addition of PPN-DBS (B) the GPe clusters are disrupted after some transients.

Capozzo et al. (2009) have reported the effect of PPN-DBS on STN cells depend on the frequency and intensity of the stimulus. PPN stimulus with low frequency (10–40 Hz) and moderate intensity (50–400 μA) has an activated working on STN neurons. Either a higher intensity or a higher frequency of the stimulus suppress the STN firing. We have only looked at low frequencies (≤ 40 Hz) and moderate intensities (10 and $100 \mu\text{A cm}^{-2}$). We observe also an activated working on STN cells. Galati et al. (2008) have shown in PD patient that PPN-DBS at 25 Hz change the mean firing of STN neurons. In particular, the firing rate of the bursting STN neurons decrease and the firing rate of the irregular and regular STN neurons increase.

In many respects, our modeling approach is a first investigation how the PPN could be integrated into a larger network. A first extension can be made by investigating how various experimentally recorded LFP's would generate input to the PPN. Here a distinction must be made between medication on and off since axial signs are unresponsive to medication in late stages of PD. For instance, Androulidakis, Khan et al. (2008); Androulidakis, Mazzone et al. (2008) found prominent 7–11 Hz oscillations in on medication states. Subsequently, Weinberger et al. (2008) found prominent beta oscillations in LFP in three PD patients off medication. Neuronal firing did not show these oscillations, rather there pattern was bursty or regular. More recently, Tsang et al. (2010) showed beta synchronization in premovement activity in the on medication state, but not in the off medication. It is important to note that these inconsistencies could be due to slightly different recording areas.

Second, one could study the effect of the output of the PPN model on receiving descending pathways and nuclei, e.g. to spinal motor neurons. For the connection to motor neurons it would be interesting whether experimental results of Pierantozzi et al. (2007) can be reproduced with our model. They hypothesize that PPN-DBS acts on spinal cord excitability improving the

reticulospinal pathway. This could be tested with the output of our model.

Further tuning of our PPN type I model according to recent data of Simon et al. (2010) should be done. This requires more about the dynamics of the ionic currents, than currently available. At present the dynamics is based on neurophysiological data of the thalamocortical relay neuron ($I_{\text{Na,leak}}$, $I_{\text{K,leak}}$, I_{Na} , I_{K} , I and I_h) and the pre-Bötzinger neuron ($I_{\text{Na,p}}$).

Acknowledgements

The authors gratefully acknowledge the support of the Brain-Gain Smart Mix Programme of the Netherlands Ministry of Economic Affairs and the Netherlands Ministry of Education, Culture and Science.

Appendix. The ionic current equations for the PPN model

We assume that $I_{\text{Na,L}}$, $I_{\text{K,L}}$, I_{Na} , I_{K} , I_h and $I_{\text{Na,p}}$ are linear functions of the membrane potential (V_m), with a ionic driving force given by the Nernst equation. These currents have the following general form:

$$I_{\text{ion}} = g_{\max} m^a h^b (V_m - E_{\text{ion}}) \quad a, b \in \mathbb{N}_0, \quad (\text{A.1})$$

where g_{\max} is the maximum ion channel conductance, m is the activation gating variable, h is the inactivation gating variable and E_{ion} is the reversal potential. The reversal potential is defined by the Nernst equation. We assume the ionic concentrations are constant during our simulations. The current–voltage relation for I_T has a non-linear dependence upon driving force that is described by the Goldman–Hodgkin–Katz current equation ($G(V_m, [\text{ion}]_i, [\text{ion}]_o)$). Thus,

$$I_T = m^2 h G(V_m, [\text{Ca}]_i, [\text{Ca}]_o)$$

with

$$G(V_m, [Ca]_i, [Ca]_o) = p_{Ca} \frac{z^2 F^2 V_m}{RT} \frac{[Ca]_i - [Ca]_o \exp\left(-\frac{zFV}{RT}\right)}{1 - \exp\left(-\frac{zFV}{RT}\right)}, \quad (\text{A.2})$$

where $p_{Ca} = 10^{-4} \text{ cm s}^{-1}$ is the maximum T-type calcium channel permeability, $z = 2$ is the valence of calcium ion, F is the Faraday's constant in $\text{J V}^{-1} \text{ mol}^{-1}$, R is the gas constant in $\text{J K}^{-1} \text{ mol}^{-1}$, $T = 309.15 \text{ K}$ is the absolute temperature, $[Ca]_o = 2 \text{ mM}$ is the extracellular Ca^{2+} concentration of the model cell. Intracellular Ca^{2+} concentration ($[Ca]_i$) depends on T-type calcium current and is given by the following equation

$$\frac{d[Ca]_i}{dt} = \frac{[Ca]_{buff} - [Ca]_i}{\tau_{Ca}} - k_{Ca} I_T,$$

where $[Ca]_{buff} = 0.00024 \text{ mM}$, $\tau_{Ca} = 5 \text{ ms}$, $k_{Ca} = 5.1821e - 5$ is a unit conversion factor.

The (in)activation gating variables in Eqs. (A.1) and (A.2) are described by differential equations of the form:

$$\frac{dX}{dt} = (X_\infty(V_m) - X)/\tau_X(V_m) \quad X = m, h$$

where $X_\infty(V_m) = \alpha_X(V_m)/(\alpha_X(V_m) + \beta_X(V_m))$ is the steady-state voltage-dependent (in)activation function of X and $\tau_X(V_m) = 1/(\alpha_X(V_m) + \beta_X(V_m))$ is the voltage-dependent time constant. These functions are based on neurophysiological data of the thalamocortical relay neuron (Destexhe et al., 1998; Huguenard & McCormick, 1992; McCormick & Huguenard, 1992), except for the persistent sodium gating variables which are based neurophysiological data of the pre-Bötzinger neuron (Rybäk, Ptak et al., 2003; Rybäk, Shevtsova et al., 2003).

Sodium and potassium leak currents

$$I_{Na,L} = g_{Na,L}(V_m - E_{Na})$$

$$I_{K,L} = g_{K,L}(V_m - E_K).$$

Sodium current

$$I_{Na} = g_{Na} m^3 h(V_m - E_{Na})$$

$$\alpha_m = 0.32(V_m + 55)/(1 - \exp(-(V_m + 55)/4))$$

$$\beta_m = -0.28(V_m + 28)/(1 - \exp((V + 28)/5))$$

$$\alpha_h = 0.12 \exp(-(V_m + 51)/18)$$

$$\beta_h = 4/(1 + \exp(-(V_m + 28)/5)).$$

Potassium current

$$I_K = g_K m^4(V_m - E_K)$$

$$\alpha_m = 0.032(V_m + 63.8)/(1 - \exp(-(V_m + 63.8)/5))$$

$$\beta_m = 0.5(\exp(-(V_m + 68.8)/40)).$$

Hyperpolarization-activated current

$$I_{hyp} = g_{hyp} m^3(V_m - E_{hyp})$$

$$m_\infty = 1/(1 + \exp((V_m + 85)/5.5))$$

$$\tau_m = 1/(\exp(-15.45 - 0.086V_m) + \exp(-1.17 + 0.0701V_m)).$$

Persistent sodium current

$$I_{Na,p} = g_{Na,p} m h(V_m - E_{Na})$$

$$m_\infty = 1/(1 + \exp(-(V_m + 47.1)/3.1))$$

$$\tau_m = 0.9/\cosh((V_m + 47.1)/6.2)$$

$$h_\infty = 1/(1 + \exp((V_m + 57)/3))$$

$$\tau_h = 20000/\cosh((V_m + 57)/6).$$

In the model, time is in ms, voltages are in mV, ion concentrations are in mM, currents are in $\mu\text{A cm}^{-2}$, conductance are in mS cm^{-2} and the membrane capacitance is in $\mu\text{F cm}^{-2}$. The membrane capacitance is assumed to be unity and the reversal potentials are set to $E_{Na} = 45$, $E_K = -95$, $E_{hyp} = -43 \text{ mV}$, the conductances to $g_{Na,L} = 0.0207$, $g_{K,L} = 0.05$, $g_{Na} = 30$, $g_K = 3.2$, $g_{hyp} = 0.4$, $g_{Na,p} = 45 \text{ mS cm}^{-2}$.

References

- Androulidakis, A. G., Khan, S., Litvak, V., Pleydell-Pearce, C. W., Brown, P., & Gill, S. S. (2008). Local field potential recordings from the pedunculopontine nucleus in a parkinsonian patient. *Neuroreport*, 19, 59–62.
- Androulidakis, A. G., Mazzone, P., Litvak, V., Penny, W., Dileone, M., Gaynor, L. M. F. D., et al. (2008). Oscillatory activity in the pedunculopontine area of patients with parkinson's disease. *Experimental Neurology*, 211, 59–66.
- Breit, S., Bouali-Benazzouz, R., Benabid, A., & Benazzouz, A. (2001). Unilateral lesion of the nigrostriatal pathway induces an increase of neuronal activity of the pedunculopontine nucleus, which is reversed by the lesion of the subthalamic nucleus in the rat. *European Journal of Neuroscience*, 14, 1833–1842.
- Brown, P. (2003). Oscillatory nature of human basal ganglia activity: relationship to the pathophysiology of parkinson's disease. *Movement Disorders*, 18, 357–363.
- Capozzo, A., Florio, T., Confalone, G., Minchella, D., Mazzone, P., & Scarnati, E. (2009). Low frequency stimulation of the pedunculopontine nucleus modulates electrical activity of subthalamic neurons in the rat. *Journal of Neural Transmission*, 116, 51–56.
- Destexhe, A., Neubig, M., Ulrich, D., & Huguenard, J. (1998). Dendritic low-threshold calcium currents in thalamic relay cells. *Journal of Neuroscience*, 18, 3574–3588.
- Dhooge, A., Govaerts, W., & Kuznetsov, Y. A. (2003). Matcont: a matlab package for numerical bifurcation analysis of odes. *ACM Transactions on Mathematical Software*, 29, 141–164.
- Ferraye, M. U., Debù, B., Fraix, V., Goetz, L., Arduin, C., Yelnik, J., et al. (2010). Effects of pedunculopontine nucleus area stimulation on gait disorders in parkinson's disease. *Brain*, 133, 205–214.
- Florio, T., Scarnati, E., Confalone, G., Minchella, D., Galati, S., Stanzione, P., et al. (2007). High-frequency stimulation of the subthalamic nucleus modulates the activity of pedunculopontine neurons through direct activation of excitatory fibres as well as through indirect activation of inhibitory pallidal fibres in the rat. *European Journal of Neuroscience*, 25, 1174–1186.
- Galati, S., Scarnati, E., Mazzone, P., Stanzione, P., & Stefani, A. (2008). Deep brain stimulation promotes excitation and inhibition in subthalamic nucleus in parkinson's disease. *Neuroreport*, 19, 661–666.
- Halliday, D. M., Rosenberg, J. R., Amjad, A. M., Breeze, P., Conway, B. A., & Farmer, S. F. (1995). A framework for the analysis of mixed time series/point process data: theory and application to the study of physiological tremor, single motor unit discharges and electromyograms. *Progress in Biophysics and Molecular Biology*, 64, 237–278.
- Hamani, C., Stone, S., Laxton, A., & Lozano, A. M. (2007). The pedunculopontine nucleus and movement disorders: anatomy and the role for deep brain stimulation. *Parkinsonism and Related Disorders*, 13, s276–s280.
- Huguenard, J. R., & McCormick, D. A. (1992). Simulation of the currents involved in rhythmic oscillations in thalamic relay neurons. *Journal of Neurophysiology*, 68, 1373–1383.
- Jankovic, J. (2008). Parkinson's disease: clinical features and diagnosis. *Journal of Neurology, Neurosurgery, and Psychiatry*, 79, 368–376.
- Jenkinson, N., Nandi, D., Muthusamy, K., Ray, N. J., Gregory, R., & Stein, J. F. (2009). Anatomy, physiology, and pathophysiology of the pedunculopontine nucleus. *Movement Disorders*, 24, 319–328.
- Kang, Y., & Kitai, S. (1990). Electrophysiological properties of pedunculopontine neurons and their postsynaptic responses following stimulation of substantia nigra reticulata. *Brain Research*, 535, 79–95.
- Kühn, A. A., Kempf, F., Brücke, C., Doyle, L. G., Martinez-Torres, I., Pogosyan, A., et al. (2008). High-frequency stimulation of the subthalamic nucleus suppresses oscillatory β activity in patients with parkinson's disease in parallel with improvement in motor performance. *The Journal of Neuroscience*, 28, 6165–6173.
- Matsumura, M., Watanabe, K., & Ohye, C. (1997). Single-unit activity in the primate nucleus segmenti pedunculopontinus related to voluntary arm movement. *Neuroscience Research*, 28, 155–165.
- Mazzone, P., Lozano, A., Stanzione, P., Galati, S., Scarnati, E., Peppe, A., et al. (2005). Implantation of human pedunculopontine nucleus: a safe and clinically relevant target in parkinson's disease. *Neuroreport*, 16, 1877–1881.
- McCormick, D. A., & Huguenard, J. R. (1992). A model of the electrophysiological properties of thalamocortical relay neurons. *Journal of Neurophysiology*, 68, 1384–1400.
- Mena-Segovia, J., Bolam, J. P., & Magill, P. J. (2004). Pedunculopontine nucleus and basal ganglia: distant relatives or part of the same family. *Trends in Neurosciences*, 27, 585–588.
- Nandi, D., Aziz, T. Z., Giladi, N., Winter, J., & Stein, J. F. (2002). Reversal of akinesia in experimental parkinsonism by gaba antagonist microinjections in the pedunculopontine nucleus. *Brain*, 125, 2418–2430.
- Nandi, D., Aziz, T. Z., Liu, X., & Stein, J. F. (2002). Brainstem motor loops in the control of movement. *Movement Disorders*, 17, s22–s27.
- Ogura, M., & Kita, H. (2000). Dynorphin exerts both postsynaptic and presynaptic effects in the globus pallidus of the rat. *Journal of Neurophysiology*, 83, 3366–3376.
- Olszewski, J., & Baxter, J. (1954). *Cytoarchitecture of the human brain stem* (1st ed.). Philadelphia, USA: Lippincott.
- Pahapill, P. A., & Lozano, A. M. (2000). The pedunculopontine nucleus and parkinson's disease. *Brain*, 123, 1767–1783.
- Pierantozzi, M., Palmieri, M. G., Galati, S., Stanzione, P., Peppe, A., Tropepi, D., et al. (2007). Pedunculopontine nucleus deep brain stimulation changes spinal cord excitability in parkinson's disease patients. *Journal of Neural Transmission*, 115, 731–735.

- Pirini, M., Rocchi, L., Sensi, M., & Chiari, L. (2009). A computational modelling approach to investigate different targets in deep brain stimulation for parkinson's disease. *Journal of Computational Neuroscience*, 26, 91–107.
- Plaha, P., & Gill, S. S. (2005). Bilateral deep brain stimulation of the pedunculopontine nucleus for parkinson's disease. *Neuroreport*, 16, 1883–1887.
- Rubin, J. E., & Terman, D. (2004). High frequency stimulation of the subthalamic nucleus eliminates pathological thalamic rhythmicity in a computational model. *Journal of Computational Neuroscience*, 16, 211–235.
- Rybak, I. A., Ptak, K., Shevtsova, N. A., & McCrimmon, D. R. (2003). Sodium currents in neurons from the rostroventrolateral medulla of the rat. *Journal of Neurophysiology*, 90, 1635–1642.
- Rybak, I. A., Shevtsova, N. A., St-John, W. M., Paton, J. F. R., & Pierrefiche, O. (2003). Endogenous rhythm generation in the pre-bötzinger complex and ionic currents: modelling and in vitro studies. *European Journal of Neuroscience*, 18, 239–257.
- Scarnati, E., Proia, A., Loreto, S. D., & Pacitti, C. (1987). The reciprocal electrophysiological influence between the nucleus tegmenti pedunculopontinus and the substantia nigra in normal and decorticated rats. *Brain Research*, 423, 116–124.
- Simon, C., Kezunovic, N., Ye, M., Hyde, J., Hayar, A., Williams, D. K., et al. (2010). Gamma band unit activity and population responses in the pedunculopontine nucleus. *Journal of Neurophysiology*, 104, 463–474.
- Stanford, I. M., & Cooper, A. J. (1999). Presynaptic μ and δ opioid receptor modulation of gaba_A ipscs in the rat globus pallidus in vitro. *The Journal of Neuroscience*, 19, 4796–4803.
- Stefani, A., Lozano, A. M., Peppe, A., Stanzone, P., Galati, S., Tropepi, D., et al. (2007). Bilateral deep brain stimulation of the pedunculopontine and subthalamic nuclei in severe parkinson's disease. *Brain*, 130, 1596–1607.
- Takakusaki, K., & Kitai, S. T. (1997). Ionic mechanisms involved in the spontaneous firing of tegmental pedunculopontine nucleus neurons of the rat. *Neuroscience*, 78, 771–794.
- Takakusaki, K., Shiroyama, T., & Kitai, S. T. (1997). Two types of cholinergic neurons in the rat tegmental pedunculopontine nucleus: electrophysiological and morphological characterization. *Neuroscience*, 79, 1089–1109.
- Takakusaki, K., Shiroyama, T., Yamamoto, T., & Kitai, S. T. (1996). Cholinergic and noncholinergic tegmental pedunculopontine projection neurons in rats revealed by intracellular labeling. *The Journal of Comparative Neurology*, 371, 345–361.
- Terman, D., Rubin, J. E., Yew, A. C., & Wilson, C. J. (2002). Activity patterns in a model for the subthalamopallidal network of the basal ganglia. *The Journal of Neuroscience*, 22, 2963–2976.
- Tsang, E., Hamani, C., Moro, E., Mazzella, F., Poon, Y., Lozano, A., et al. (2010). Involvement of the human pedunculopontine nucleus region in voluntary movements. *Neurology*, 75.
- Weinberger, M., Hamani, C., Hutchison, W. D., Moro, E., Lozano, A. M., & Dostrovsky, J. O. (2008). Pedunculopontine nucleus microelectrode recordings in movement disorder patients. *Experimental Brain Research*, 188, 165–174.